

## Geometric control and memory in networks of hysteretic elements Shohat, D.; Hecke, M.L. van

## Citation

Shohat, D., & Hecke, M. L. van. (2025). Geometric control and memory in networks of hysteretic elements. *Physical Review Letters*, 134(18). doi:10.1103/PhysRevLett.134.188201

Version: Publisher's Version

License: <u>Licensed under Article 25fa Copyright Act/Law (Amendment Taverne)</u>

Downloaded from: <a href="https://hdl.handle.net/1887/4283643">https://hdl.handle.net/1887/4283643</a>

**Note:** To cite this publication please use the final published version (if applicable).

## Geometric Control and Memory in Networks of Hysteretic Elements

Dor Shohat<sup>1,2</sup> and Martin van Hecke<sup>2,3</sup>

<sup>1</sup>Department of Condensed Matter, School of Physics and Astronomy, Tel Aviv University, Tel Aviv 69978, Israel

<sup>2</sup>AMOLF, Science Park 104, 1098 XG Amsterdam, The Netherlands

<sup>3</sup>Huygens-Kamerling Onnes Lab, Universiteit Leiden, PObox 9504, 2300 RA Leiden, The Netherlands

(Received 13 September 2024; accepted 4 April 2025; published 6 May 2025)

The response of driven frustrated media stems from interacting hysteretic elements. We derive explicit mappings from networks of hysteretic springs to their abstract representation as interacting hysterons. These mappings reveal how the physical network controls the signs, magnitudes, symmetries, and pairwise nature of the hysteron interactions. In addition, strong geometric nonlinearities can produce pathways that require excess hysterons or even break hysteron models. Our results pave the way for metamaterials with geometrically controlled interactions, pathways, and functionalities, and highlight fundamental limitations of abstract hysterons in modeling disordered systems.

DOI: 10.1103/PhysRevLett.134.188201

The response of driven disordered media, such as compressed crumpled sheets or sheared amorphous solids, forms pathways composed of sequential transitions between metastable states [1–5]. These pathways encode memories of past driving [6], including its direction [7] and amplitude [8–11], and even computational capabilities [4,12–14]. Understanding the connections between properties of a physical system and its pathways is crucial, both for the fundamental understanding of amorphous solids [1,2,15,16], and for devising (meta)materials with targeted pathways, memory effects, or *in materia* computational capabilities [13,17–20].

Physically, these pathways are often composed of successive flips of localized hysteretic elements such as beams, ridges, or particle clusters, which function as "material bits" [3–5,18,21]. Therefore, strictly binary hysteretic elements, known as hysterons [22,23], are prime candidates for modeling and designing memory effects and pathways [1,24–27] [Figs. 1(a) and 1(b)]. The strength of hysteron models is that they condense physical systems into a small set of parameters (switching thresholds) which characterize the material bits and their interactions [23,24]. However, we lack a general link between these parameters and the underlying physics. Materializing targeted pathways from the hysteron model remains a challenge [13,28], while random hysteron parameters can produce nonphysical responses or become ill defined [23,26,29]. Can we use hysteron models to describe and design physical systems composed of hysteretic elements?

To address these questions, we consider physical networks of hysteretic springs, and derive explicit mappings to the switching thresholds of the hysteron model [Fig. 1(c)]. For linear geometries, we map hysteretic spring networks to hysterons with pairwise interactions; for two-dimensional networks, this mapping produces geometrically tunable,

nonpairwise interactions. We leverage this geometric control to realize exotic pathways, including multiperiodic orbits where the systems only returns to its initial state after multiple driving cycles [25,30]. However, when springs align or orient perpendicular to the drive, this mapping requires more hysterons than springs or may even break

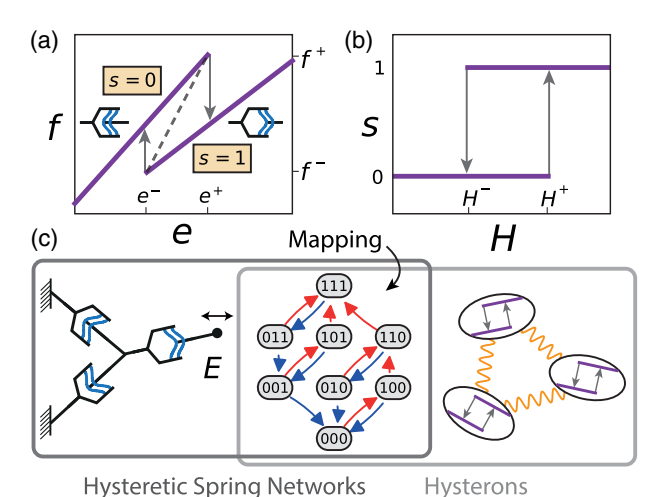


FIG. 1. (a) Force-displacement curve for a hysteretic spring with two linear branches (purple); pictograms represent the configurations of a physical realization [13]. (b) The binary phase s := 0, 1 of a hysteron as a function of the external field H. (c) Relation between networks of hysteretic springs driven by displacement E (left) and interacting hysteron models (right). Under certain conditions, networks and hysterons can be precisely mapped and produce the same transition graph (center); however, in other cases, springs may follow nonhysteron pathways and vice versa. In the t-graph, states are represented with

binary strings, and transitions with red (blue) arrows for increas-

ing (decreasing) external driving.

down: exceptional networks can exhibit pathways beyond those of the hysteron framework.

Our Letter conveys two key insights. First, as exceptional alignment is unavoidable in large disordered systems, it may lead to discrepancies with hysteron models, and we identify key ingredients to improve mesoscopic models for amorphous media. Second, our Letter provides a precise, geometric, and general strategy to materialize targeted pathways in specific networks of hysteretic elements, whether electronic [31–33], pneumatic [34,35], fluidic [36], or mechanical [17,18,28]. This paves the way for rationally designed (meta)materials with on-demand memories and computational capabilities [16,19,20,37].

Hysteretic springs, pathways, and t-graphs—We consider hysteretic elements, characterized by a bilinear relation between two conjugate physical variables, such as current and voltage [31–33], pressure and volume or flow [34–36], or, as we use here, force  $f_i$  and displacement  $e_i$  [13,38]:

$$f_i = (k_i^0 + \Delta k_i s_i) e_i - g_i s_i. \tag{1}$$

Each hysteretic spring switches between its two phases  $s_i = 0$  and  $s_i = 1$  when its displacement  $e_i$  exceeds the local, hysteretic switching thresholds  $e_i^+ > e_i^-$ ; the stiffness of its branches are  $k_i^0$  and  $k_i^1 := k_i^0 + \Delta k_i$ , and  $g_i$  sets the force jumps between branches [Fig. 1(a)] [39].

We connect n of these springs in a network and follow their response to edge-applied driving by controlling the overall deformation E. We assume no simultaneous flips. and focus on slow driving with overdamped dynamics [Fig. 1(c)]; other conditions, including spatially textured driving [4,17], race conditions [23], and dynamic driving [42,43] introduce additional complexity. The response is piecewise smooth, but when  $e_i$  reaches its individual switching thresholds, the *ith* element flips its phase  $s_i$ : 0  $\leftrightarrow$  1. These events cause a rapid change in the forces and extensions, which in turn may trigger additional flips (avalanches). The critical values of E where transitions are triggered define the global, state-dependent switching thresholds  $E_i^{\pm}(S)$ , where  $S := (s_1, s_2, ...)$ . The transitions and switching thresholds can be collected in the transition graph (t-graph), which captures the response to any sequential driving protocol and encodes the memory capacity and capabilities [Fig. 1(c)] [1,4,23,44].

Hysteron model—A simplified description of such networks—and complex media in general—is provided by hysterons, abstracted hysteretic elements which are purely binary, and driven by an external field H [23–25] [Fig. 1(b)]. A collection of interacting hysterons is defined by the switching thresholds  $H_i^{\pm}(S)$  which specify when hysteron i flips between phases  $s_i = 0$ , 1, and which determine the t-graph [23,24,26]. Often, the state-dependent thresholds are modeled via pairwise interactions:

$$H_i^{\pm}(S) = h_i^{\pm} - \sum_j c_{ij}^{\pm} s_j, \text{ with } c_{ii}^{\pm} = 0,$$
 (2)

where  $h_i^{\pm}$  are the fixed bare thresholds and  $c_{ij}^{\pm}$  are interaction coefficients [4,13,23]. Hysteron models lack a physical description for these parameters and typically assign them randomly [25–27,30]; however, for specific parameters, race conditions and unphysical loops may occur [29].

Interactions and mapping—A successful mapping between a network and the hysteron model requires that they exhibit the same pathways and the same switching thresholds. In hysteretic spring networks, interactions are mediated by physical balance equations, e.g., force balance. The switching thresholds can then be determined as follows: (i) freeze the state S so that the force-displacement relations  $f_i(e_i)$  are strictly linear; (ii) use force balance to determine  $e_i$  as a function of the driving E; and (iii) determine state-dependent switching thresholds  $E_i^\pm(S)$  by calculating the values of E where  $e_i=e_i^\pm$  (either analytically or numerically). Once  $E_i^{\pm}(S)$  is determined, we can trivially identify these with  $H_i^{\pm}(S)$ , and then determine whether the interactions are pairwise, top-down symmetric (i.e.,  $c_{ii}^+ = c_{ii}^-$ ), and their precise values. Hence, our goal is to map a given geometry of springs with their parameters to the switching thresholds  $E_i^{\pm}(S)$ .

Linear networks—We first consider mechanical hysteretic springs in serial or parallel geometries: these can be mapped onto interacting hysterons [Fig. 2(a)]. The corresponding force balance equations are scalar and produce pairwise interactions [see Eq. (2)]. These can be worked out explicitly from the collective force-displacement curves F(E,S) [Fig. 2(b)] [39]. For serial coupling and controlled total displacement  $E = \sum e_i$  [45] we obtain

$$c_{ij}^{\pm} = -\frac{g_j}{nk_j^1} + \frac{\Delta k_j}{nk_j^0 k_j^1} f_i^{\pm}.$$
 (3)

For parallel coupling, an additional spring of stiffness K mediates the interactions [46], and we obtain

$$c_{ij}^{\pm} = \frac{g_j - \Delta k_j e_i^{\pm}}{K}.\tag{4}$$

These expressions reveal how geometry controls the interactions: serial coupling leads to negative interactions  $(c_{ij} < 0)$  [13], while parallel coupling leads to positive interactions  $(c_{ij} > 0)$ . For stiffness-symmetric springs  $(\Delta k = 0)$ , interactions are up-down symmetric  $(c_{ij}^+ = c_{ij}^-)$  and global, i.e., each hysteron affects all others equally  $(c_{ij} = c_{kj})$ . In contrast, for  $\Delta k \neq 0$  this symmetry is broken —as seen in experiments [4]—with large  $\Delta k$  producing opposite signs of  $c_{ij}^+$  and  $c_{ij}^-$  [Figs. 2(b) and 2(d)].

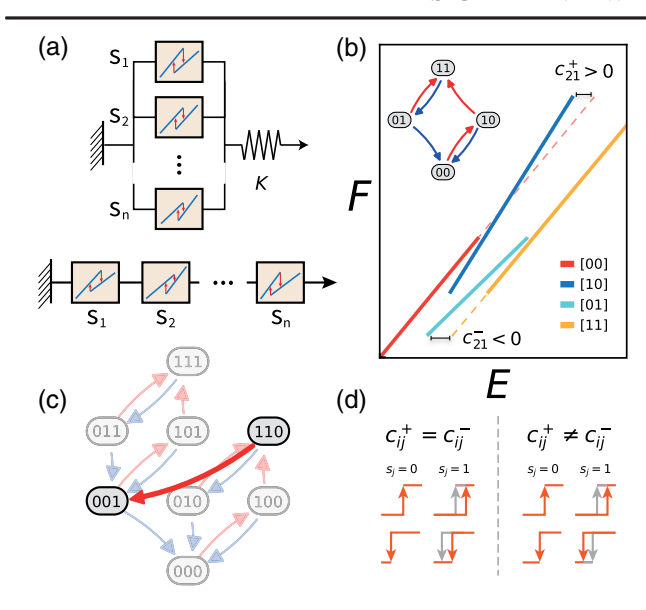


FIG. 2. (a) Hysteretic springs under controlled deformations interact when coupled in parallel (spring K mediates interactions, top) or in series (bottom). (b) Collective response curves F(E,S) for two serially coupled hysteretic springs, with endpoints representing state dependent switching thresholds. The interaction coefficients follow from comparing appropriate pairs of branches, e.g.,  $c_{21}^+ = E[f_2^+, (00)] - E[f_2^+, (01)]$  and  $c_{21}^- = E[f_2^-, (01)] - E[f_2^-, (11)]$ . Here these have opposite signs. Inset: corresponding t-graph. (c) T-graph featuring a dissonant avalanche (See Ref. [39] for details and parameters). (d) Interactions that respect (left) and break (right) the up or down symmetry  $c_{ij}^+ = c_{ij}^-$  (arrows represent switching thresholds: orange, bare; gray, with interactions).

These interactions control the pathways of the network. Interactions may produce avalanches whose sequences of up  $(u:0 \to 1)$  and down  $(d:1 \to 0)$  flips follow the signs of  $c_{ii}^{\pm}$ : (i) in serial coupling of symmetric hysteretic springs  $(\Delta k = 0)$ , negative interactions produce avalanches that alternate between u and d and are of maximal length two [13]; (ii) stiffness-asymmetric springs can produce exotic, "dissonant" avalanches like duu, where a decrease in E (or H) leads to an increase in the magnetization  $m := \sum_i s_i$  or vice versa [47] [Fig. 2(d)] [23]; (iii) in parallel coupling, positive interactions drive monotonic avalanches (only u's or d's) of arbitrary length. Recently, countersnapping springs have been realized—where up (down) instabilities counterintuitively lead to force jumps (drops) as opposed to ordinary hysteretic springs [48–50]. Such countersnapping springs can be captured in our framework by controlling the signs of  $g_i^{\pm}$ , and can produce monotonic avalanches in serial geometries, and alternating avalanches in parallel geometries [39].

Nevertheless, the range of pathways in linear networks is limited. This is because all elements experience the same force (displacement) in serial (parallel) networks, so that their switching thresholds follow a fixed order set by the individual switching forces  $f_i^{\pm}$  (displacements  $e_i^{\pm}$ ) [13].

For example, if in a serial network  $f_i^+ < f_j^+$ , then hysteron i will always flip up before hysteron j.

This limitation is reflected in the qualitative features of the *t*-graphs, which in particular cannot sustain a multiperiodic response. We explore them numerically for three hysteretic elements in linear networks [13,23], and find that out of hundreds of *t*-graphs, the vast majority obeys a hierarchical structure of nested loops known as loop-return point memory (I-RPM) [51], which hinders the emergence of complex behavior [39]. Hence, while the sign and magnitude of interactions can be controlled, linear geometries severely limit the range of pathways and memory effects.

2D networks—Our understanding of the linear geometries suggests that 2D networks of hysteretic elements may open a route to more advanced pathways and memory effects. We consider the paradigmatic case of a trigonal hub, where the two fixed and one moving corner of a triangle  $\vec{r}_i = (x_i, y_i)$  connect to a central, freely moving point  $\vec{M}$  via three symmetric hysteretic springs with  $k_i = 1$ [Fig. 3(a)]. We deform the hub by slowly driving  $H = x_1$ . Since the force balance on  $\vec{M}$  is vectorial and angle dependent, the flipping order is no longer subordinate to the ordering of  $f_i^{\pm}$  or  $e_i^{\pm}$ , allowing a far greater range of pathways, including multiperiodic responses. We use this vectorial force balance to derive exact expressions for the interaction coefficients, and find that the ratio  $g/e^{\pm}$ determines their form. For small  $g/e^{\pm}$ , the interactions are pairwise and controlled by the angles between the springs, while for large  $g/e^{\pm}$ , geometric nonlinearities produce nonpairwise interactions and can even lead to a breakdown of the mapping from springs to hysterons.

When  $g/e^{\pm} \ll 1$ , the changes in angles following an instability are small, and the interactions can be expressed geometrically:

$$c_{ij}^{\pm} \approx z_i g_j \frac{\cos \varphi_{ij}}{\cos \theta_i},$$
 (5)

where the geometrical factor  $z_i$  arises from the connectivity of the trigonal hub  $([z_1,z_2,z_3]=[\frac{1}{2},1,1]), \, \varphi_{ij}$  is the angle between  $s_i$  and  $s_j$ , and all angles are evaluated at the instability of hysteron i. This expression has a clear geometrical interpretation. First, the jump between the branches,  $g_j$ , provides the typical scale for the strength of interactions, as in the linear networks. Second, the factor  $1/\cos\theta_i$  represents how global driving is coupled to stretching of hysteron i. Third, the factor  $\cos\varphi_{ij}$  captures the geometric coupling: consistent with our findings for serial and parallel couplings, this factor approaches 1(-1) for  $\varphi_{ij}=0$  ( $\varphi_{ij}=\pi$ ), and approaches zero for perpendicular hysterons.

When  $g/e^{\pm} \not\ll 1$ , the angle changes during flipping events are significant. Interactions are neither pairwise nor

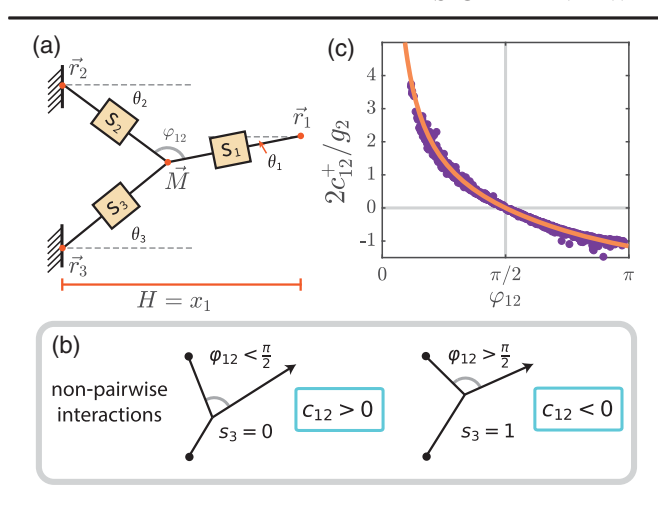


FIG. 3. (a) Trigonal hub with hysterons connected in 2D.  $\vec{r}_1$  is externally pulled along the  $\hat{x}$  axis. (b) Strong nonpairwise interactions, where flipping  $s_3$  reverses the interactions between hysterons one and two. (c) Comparison of the numerically obtained  $c_{12}^+$  (dots) and approximate expression, Eq. (5) (light curve), for  $10^4$  random samples; here we have assumed the geometrical relation  $\theta_1 = \pi/2 - 2\varphi_{12}/3$  [39].

up-down symmetric, and depend on the initial states. For example,  $c_{12}^{\pm}$  will depend on the phase of  $s_3$  [39]. Yet, Eq. (5) still holds geometrical intuition: e.g., flipping  $s_3$  may change  $\varphi_{12}$ . If as a result  $\varphi_{12}$  crosses  $\pi/2$ ,  $c_{12}^{+}(s_3=0)$  and  $c_{12}^{+}(s_3=1)$  have opposite signs, presenting a strong deviation from pairwise interactions [Fig. 3(b); see the Supplemental Material [39], Video 1].

We complement our analytical analysis with numerical simulations, where we determine  $\vec{M}$  using overdamped dynamics:  $\dot{\vec{M}} = \gamma^{-1} \sum_i \vec{f}_i$ , where  $\gamma$  is a large damping constant and the forces are given by Eq. (1). Starting from any state S we quasistatically drive H, follow  $\vec{M}$ , and identify instabilities whenever  $e_i = e_i^{\pm}$ . We find that the numerically calculated interaction coefficient  $c_{12}^+$  closely matches the geometrical expression [Eq. (5)] [Fig. 3(c)] [39].

2D t-graphs—The range of t-graphs that can be realized by 2D networks is huge, and we use our numerical scheme to generalize earlier t-graph sampling protocols [13,23] to explore their diversity. First, we find that the trigonal hub can easily host multiperiodic cycles with a periodicity T=2 (Fig. 4; see the Supplemental Material [39], Video 2). Such cycles are a hallmark of complex behavior in driven amorphous systems, break 1-RPM, and cannot be realized in linear geometries (because their switching thresholds follow a fixed order).

Second, the trigonal hub produces pathways where starting from a certain stable state S, either increasing or decreasing the drive H, triggers the same transition. This violates the assumption of all hysteron models that transitions under increased (decreased) driving are initiated by a hysteretic element flipping up (down). However, this effect can easily be understood geometrically, and is a

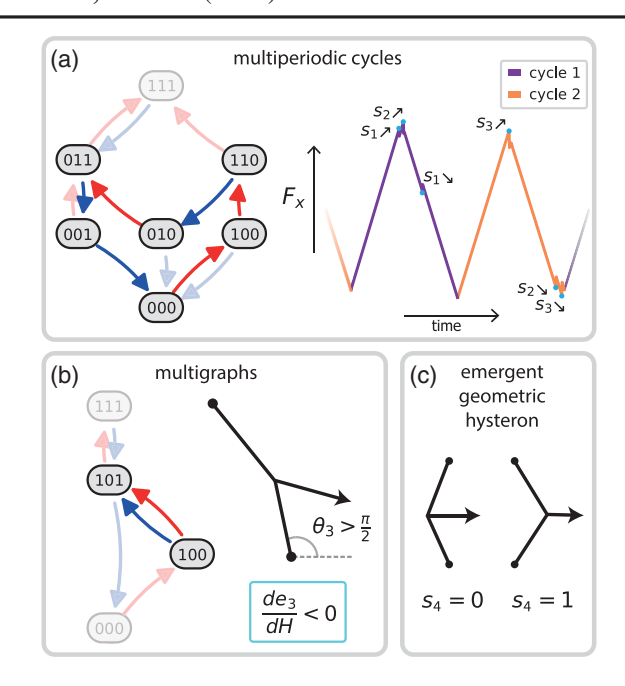


FIG. 4. (a) T-graph showing a multiperiodic cycle with periodicity T=2 (left): starting from state (000) and driving H cyclically, the system returns to (000) after T=2 driving cycles [39]. Multiperiodicity is also apparent in the mechanical response (right), the force  $F_x$  measured at  $\vec{r}_1$  as a function of time. (b) Multigraph (left): starting from (100), either increasing or decreasing H leads to the same transition  $s_3=0 \to 1$ ; this happens when  $e_3$  is perpendicular to the driving. Decreasing H stretches  $e_3$  if  $\theta_3 > \pi/2$  (right). (c) Illustration of an emergent, geometric 4th hysteron. The state  $S=(s_1,s_2,s_3)$  is fixed while the hub exhibits global, bistable buckling.

general feature of higher dimensional networks: if the angle  $(\theta_i)$  between a spring and the driving H is around  $\pi/2$ , both an increase and a decrease of H can lead to stretching of this spring thus triggering the same flipping [Eq. (5)]. The corresponding t-graph is a multigraph, where multiple directed transitions connect the same two states [Fig. 4(b); see the Supplemental Material [39], Video 3] [52]. Similarly, both for  $H \to \infty$  and  $H \to -\infty$ , the springs get stretched and all switch to phase 1—hence, there is no guarantee that the springs will ever reach  $s_i = 0$ .

Third, 2D networks can give rise to additional hysteretic degrees of freedom associated with buckling [Fig. 4(c)]. This geometric degree of freedom can be mapped to an additional (fourth) hysteron, for example by defining its phase via the leaning direction of the buckled structure [43]. Such geometric hysterons produce a wide variety of t-graphs [39].

For large random networks, we expect the numbers of springs perpendicular to the driving and of emergent hysterons to proliferate [53]. This suggests that for increasingly large systems, the mapping from spring networks to hysteron models progressively fails.

Conclusion and outlook—Networks of hysteretic elements allow one to investigate the links between real space

configurations and abstract hysteron models. We have shown how geometry controls interactions, leading to a general, geometric strategy to materialize targeted pathways in networks of hysteretic elements. At the same time, the exceptional 2D geometries clarify that spurious alignment between elements and between elements and driving, may break the description of physical systems by hysteron models. In large networks, these effects could potentially be enhanced by nonaffine deformations [54]. This breakdown implies that previous insights on the mechanics of amorphous solids, derived from hysteron models, may require reconsideration; point toward the importance of exceptionally aligned geometries for future descriptions of amorphous solids [15,24,38,55]; and suggest that physical systems exhibit a wider range of responses and memory effects than shown in the hysteron model [17,21].

While we focused here on controlled deformations, slow driving, and nondegenerate conditions, we note that stress control (instead of strain) [21], textured driving [4,17], dynamic driving [42,43], or race conditions [23] can significantly extend the range of physically realizable pathways, and further probe the validity of hysteron models [26,43].

We briefly mention directions for future research. First, straightforward extensions include networks of mechanical elements with other hysteretic degrees of freedom (e.g., shear or rotation) [19,28,56]. Second, the complex, nonpairwise interactions in 2D networks may provide a route to understanding the emergence of glassy dynamics in large networks [57–59]. Third, physical hysteretic elements prohibit the occurrence of spurious loops, where after an instability, the system cannot find a stable state but instead gets trapped in an infinite cycle [29]. Such loops overwhelm hysterons with arbitrary switching thresholds [23,25,26], and also arise in coupled spin models [60]. Hence, physical models allow one to define ensembles of hysterons that lead to well-defined dissipative behaviors. Finally, our explicit expressions for the geometrically controlled interactions suggest that solving the inverse problem, i.e., translating a targeted pathway, t-graph, or set of switching thresholds to a specific network, is now within reach.

Acknowledgments—We thank Yoav Lahini, Paul Baconnier, Lishuai Jin, Colin Meulblok, and Margot Teunisse for insightful discussions. We are also grateful to Muhittin Mungan and Yair Shokef for a careful reading of the manuscript. This work was funded by the European Research Council Grant No. ERC-101019474. D. S. acknowledges support from the Clore Israel Foundation.

- [2] I. Regev, I. Attia, K. Dahmen, S. Sastry, and M. Mungan, Topology of the energy landscape of sheared amorphous solids and the irreversibility transition, Phys. Rev. E 103, 062614 (2021).
- [3] N. C. Keim, J. Hass, B. Kroger, and D. Wieker, Global memory from local hysteresis in an amorphous solid, Phys. Rev. Res. 2, 012004 (2020).
- [4] H. Bense and M. van Hecke, Complex pathways and memory in compressed corrugated sheets, Proc. Natl. Acad. Sci. U.S.A. 118, e2111436118 (2021).
- [5] D. Shohat, D. Hexner, and Y. Lahini, Memory from coupled instabilities in unfolded crumpled sheets, Proc. Natl. Acad. Sci. U.S.A. 119, e2200028119 (2022).
- [6] N. C. Keim, J. D. Paulsen, Z. Zeravcic, S. Sastry, and S. R. Nagel, Memory formation in matter, Rev. Mod. Phys. 91, 035002 (2019).
- [7] K. Galloway, E. Teich, X. Ma, C. Kammer, I. Graham, N. Keim, C. Reina, D. Jerolmack, A. Yodh, and P. Arratia, Relationships between structure, memory and flow in sheared disordered materials, Nat. Phys. 18, 565 (2022).
- [8] N. C. Keim and S. R. Nagel, Generic transient memory formation in disordered systems with noise, Phys. Rev. Lett. 107, 010603 (2011).
- [9] J. D. Paulsen, N. C. Keim, and S. R. Nagel, Multiple transient memories in experiments on sheared non-Brownian suspensions, Phys. Rev. Lett. 113, 068301 (2014).
- [10] S. Mukherji, N. Kandula, A. K. Sood, and R. Ganapathy, Strength of mechanical memories is maximal at the yield point of a soft glass, Phys. Rev. Lett. 122, 158001 (2019).
- [11] D. Shohat and Y. Lahini, Dissipation indicates memory formation in driven disordered systems, Phys. Rev. Lett. **130**, 048202 (2023).
- [12] L. J. Kwakernaak and M. van Hecke, Counting and sequential information processing in mechanical metamaterials, Phys. Rev. Lett. **130**, 268204 (2023).
- [13] J. Liu, M. Teunisse, G. Korovin, I. R. Vermaire, L. Jin, H. Bense, and M. van Hecke, Controlled pathways and sequential information processing in serially coupled mechanical hysterons, Proc. Natl. Acad. Sci. U.S.A. 121, e2308414121 (2024).
- [14] B. Treml, A. Gillman, P. Buskohl, and R. Vaia, Origami mechanologic, Proc. Natl. Acad. Sci. U.S.A. 115, 6916 (2018).
- [15] D. Kumar, S. Patinet, C. E. Maloney, I. Regev, D. Vandembroucq, and M. Mungan, Mapping out the glassy landscape of a mesoscopic elastoplastic model, J. Chem. Phys. **157**, 174504 (2022).
- [16] J. D. Paulsen and N. C. Keim, Mechanical memories in solids, from disorder to design, Annu. Rev. Condens. Matter Phys. 16, 61 (2024).
- [17] C. Sirote-Katz, D. Shohat, C. Merrigan, Y. Lahini, C. Nisoli, and Y. Shokef, Emergent disorder and mechanical memory in periodic metamaterials, Nat. Commun. 15, 4008 (2024).
- [18] J. Ding and M. van Hecke, Sequential snapping and pathways in a mechanical metamaterial, J. Chem. Phys. 156, 204902 (2022).
- [19] L. P. Hyatt and R. L. Harne, Programming metastable transition sequences in digital mechanical materials, Extreme Mech. Lett. **59**, 101975 (2023).

M. Mungan, S. Sastry, K. Dahmen, and I. Regev, Networks and hierarchies: How amorphous materials learn to remember, Phys. Rev. Lett. 123, 178002 (2019).

- [20] A. El Elmi and D. Pasini, Tunable sequential pathways through spatial partitioning and frustration tuning in soft metamaterials, Soft Matter 20, 1186 (2024).
- [21] T. Jules, A. Reid, K. E. Daniels, M. Mungan, and F. Lechenault, Delicate memory structure of origami switches, Phys. Rev. Res. **4**, 013128 (2022).
- [22] F. Preisach, Über die magnetische nachwirkung, Z. Phys. **94**, 277 (1935).
- [23] M. van Hecke, Profusion of transition pathways for interacting hysterons, Phys. Rev. E 104, 054608 (2021).
- [24] C. W. Lindeman and S. R. Nagel, Multiple memory formation in glassy landscapes, Sci. Adv. 7, eabg7133 (2021).
- [25] N. C. Keim and J. D. Paulsen, Multiperiodic orbits from interacting soft spots in cyclically sheared amorphous solids, Sci. Adv. 7, eabg7685 (2021).
- [26] M. H. Teunisse and M. van Hecke, Transition graphs of interacting hysterons: Structure, design, organization and statistics, arXiv:2404.11344.
- [27] C. W. Lindeman, T. R. Jalowiec, and N. C. Keim, Generalizing multiple memories from a single drive: The hysteron latch, Sci. Adv. 11, eadr5933 (2025).
- [28] J. D. Paulsen, Mechanical hysterons with tunable interactions of general sign, report, arXiv:2409.07726.
- [29] P. Baconnier, M. H. Teunisse, and M. van Hecke, Proliferation and prevention of self-loops in ensembles of interacting binary elements, arXiv:2412.12658.
- [30] A. Szulc, M. Mungan, and I. Regev, Cooperative effects driving the multi-periodic dynamics of cyclically sheared amorphous solids, J. Chem. Phys. 156, 164506 (2022).
- [31] D. B. Strukov, G. S. Snider, D. R. Stewart, and R. S. Williams, The missing memristor found, Nature (London) **453**, 80 (2008).
- [32] T. Emmerich, Y. Teng, N. Ronceray, E. Lopriore, R. Chiesa, A. Chernev, V. Artemov, M. Di Ventra, A. Kis, and A. Radenovic, Nanofluidic logic with mechano-ionic memristive switches, National electronics review 7, 271 (2024).
- [33] Y. Yeo, Y. Sharaby, N. Roy, N. Raab, K. Watanabe, T. Taniguchi, and M. Ben Shalom, Polytype switching by super-lubricant van der Waals cavity arrays, Nature (London) 638, 389 (2025).
- [34] G. Muhaxheri and C. D. Santangelo, Bifurcations of inflating balloons and interacting hysterons, Phys. Rev. E 110, 024209 (2024).
- [35] A. Djellouli, B. Van Raemdonck, Y. Wang, Y. Yang, A. Caillaud, D. Weitz, S. Rubinstein, B. Gorissen, and K. Bertoldi, Shell buckling for programmable metafluids, Nature (London) 628, 545 (2024).
- [36] A. Martínez-Calvo, M. D. Biviano, A. H. Christensen, E. Katifori, K. H. Jensen, and M. Ruiz-García, The fluidic memristor as a collective phenomenon in elastohydrodynamic networks, Nat. Commun. 15, 3121 (2024).
- [37] T. Yang, D. Hathcock, Y. Chen, P. L. McEuen, J. P. Sethna, I. Cohen, and I. Griniasty, Bifurcation instructed design of multistate machines, Proc. Natl. Acad. Sci. U.S.A. 120, e2300081120 (2023).

- [38] G. Puglisi and L. Truskinovsky, Mechanics of a discrete chain with bi-stable elements, J. Mech. Phys. Solids 48, 1 (2000).
- [39] See Supplemental Material at http://link.aps.org/supplemental/10.1103/PhysRevLett.134.188201 for detailed analytical derivations, definitions, statistics, and simulation parameters, which includes Refs. [40,41].
- [40] A. Meeussen and M. van Hecke, Multistable sheets with rewritable patterns for switchable shape-morphing, Nature (London) **621**, 516 (2023).
- [41] M. M. Terzi and M. Mungan, State transition graph of the Preisach model and the role of return-point memory, Phys. Rev. E **102**, 012122 (2020).
- [42] T. Jules, L. Michel, A. Douin, and F. Lechenault, When the dynamical writing of coupled memories with reinforcement learning meets physical bounds, Commun. Phys. 6, 25 (2023).
- [43] C. W. Lindeman, V. F. Hagh, C. I. Ip, and S. R. Nagel, Competition between energy and dynamics in memory formation, Phys. Rev. Lett. 130, 197201 (2023).
- [44] J. D. Paulsen and N. C. Keim, Minimal descriptions of cyclic memories, Proc. R. Soc. A 475, 20180874 (2019).
- [45] Serially coupled hysterons do not experience interactions under controlled force *F* [13].
- [46] For  $K \to \infty$ , parallel hysterons under controlled E are noninteracting, and under controlled F can be mapped to serially coupled hysterons under controlled E.
- [47] Crucially, the dissonant avalanches here are sequential. If the first hysteron triggers more than one flip, we consider the avalanche ill-defined due to race conditions [23].
- [48] Z. G. Nicolaou and A. E. Motter, Mechanical metamaterials with negative compressibility transitions, Nat. Mater. 11, 608 (2012).
- [49] Z. G. Nicolaou, F. Jiang, and A. E. Motter, Metamaterials with negative compressibility highlight evolving interpretations and opportunities, Nat. Commun. 15, 8573 (2024).
- [50] P. Ducarme, B. Weber, M. van Hecke, and J. Overvelde, Exotic mechanical properties enabled by countersnapping instabilities, Proc. Natl. Acad. Sci. U.S.A. 122, e2423301122 (2025).
- [51] M. Mungan and M. M. Terzi, The structure of state transition graphs in systems with return point memory: I. general theory, in *Annales Henri Poincaré* (Springer, New York, 2019), Vol. 20, pp. 2819–2872.
- [52] Multigraphs can occur in abstract hysteron models via avalanches [23], but here neither of the multitransitions are avalanches.
- [53] T. Pettinari, G. During, and E. Lerner, Elasticity of self-organized frustrated disordered spring networks, Phys. Rev. E **109**, 054906 (2024).
- [54] W. G. Ellenbroek, Z. Zeravcic, W. van Saarloos, and M. van Hecke, Non-affine response: Jammed packings vs. spring networks, Europhys. Lett. **87**, 34004 (2009).
- [55] A. Nicolas, E. E. Ferrero, K. Martens, and J.-L. Barrat, Deformation and flow of amorphous solids: Insights from elastoplastic models, Rev. Mod. Phys. 90, 045006 (2018).
- [56] L. M. Kamp, M. Zanaty, A. Zareei, B. Gorissen, R. J. Wood, and K. Bertoldi, Reprogrammable sequencing for physically intelligent under-actuated robots, arXiv:2409.03737.

- [57] D. Shohat, Y. Friedman, and Y. Lahini, Logarithmic aging via instability cascades in disordered systems, Nat. Phys. **19**, 1890 (2023).
- [58] D. Shohat, Y. Lahini, and D. Hexner, Emergent marginality in frustrated multistable networks, J. Chem. Phys. **162**, 114505 (2025).
- [59] D. Shohat, P. Baconnier, I. Procaccia, M. van Hecke, and Y. Lahini (to be published).
- [60] H. Eissfeller and M. Opper, Mean-field Monte Carlo approach to the Sherrington-Kirkpatrick model with asymmetric couplings, Phys. Rev. E **50**, 709 (1994).